J Solid State Electrochem (2011) 15:1041–1048
DOI 10.1007/s10008-011-1348-1

ORIGINAL PAPER

Ultrasound technique as a tool for high-rate incorporation of Al_2O_3 in NiCo layers

Dagmar Dietrich · Ingolf Scharf · Daniela Nickel · Lei Shi · Thomas Grund · Thomas Lampke

Received: 7 January 2011 / Revised: 10 February 2011 / Accepted: 17 February 2011 / Published online: 1 March 2011

Abstract NiCo–Al_2O_3 composite coatings were prepared by electrodeposition in a sulfamate plating bath containing Al_2O_3 particles to be co-deposited under sonication. For reliable determination of the microstructure, detailed studies on composite cross-sections were carried out by energy-dispersive spectrometer (matrix composition, particle content) and FE-SEM/electron backscattered diffraction data (particle distribution, grain size), accompanied by XRD analyses concerning texture, lattice parameter, grain size, and residual stress. The NiCo matrix with a Co/Co + Ni ratio up to 0.4 is a face-centered cubic solid solution with <100> and <110> fiber textures. The distribution of the particles (size 250 nm) was well-dispersed and enhanced up to 15 wt.% by ultrasound application during plating. Vickers hardness increased up to 50% by dispersion hardening. First-order residual stress in the matrix increased with rising Co content, thus decreasing wear resistance and revealing the complex of composite properties with partially opposite effects.

Keywords Electro-co-deposition · Ultrasound · Composites · Cross-section · Microstructure · Residual stress · Microhardness · Wear

D. Dietrich (✉) · I. Scharf · D. Nickel · L. Shi · T. Grund · T. Lampke
Institute of Materials Science and Engineering,
Chemnitz University of Technology,
09107 Chemnitz, Germany
e-mail: dagmar.dietrich@mb.tu-chemnitz.de

Introduction

Particle-reinforced metal matrix composites (MMCs) are widely applied in different fields due to their enhanced mechanical and tribological properties by dispersion hardening or self-lubrication, improved chemical and temperature inertness, as well as for special applications like photocatalytic effects [1]. Besides bulk material, also MMC coatings are known. Generally, they can be fabricated by diverse methods such as electrodeposition [2], hot pressing [3], thermal spraying [4], and cold spraying [5]. Among these methods, electrodeposition has been considered to be a technologically feasible and economically superior technique for producing composite coatings at low costs, which can be performed at normal pressure and ambient temperature. Electrodeposition yields high deposition rates and offers the capability to handle complex geometries.

It is well known that the improved properties of the composites depend on the content and the degree of dispersion of the incorporated particles. Many approaches and techniques have been utilized to improve the content and degree of particle dispersion in the metal matrix, such as sediment co-deposition [6], changing the type of the applied current [7], adding organic surfactants in the electrolyte [8], or applying ultrasound [9–12]. Among these methods, it has been recognized that the ultrasound treatment has a considerable potential for being used on an industrial scale. Furthermore, using ultrasound can cause desirable effects on the electrochemical process like increased brightness and hardness, improved adhesion to

the substrate, and a finer grain size. Lampke et al. [9] studied in detail the influence of a 35-kHz ultrasound bath on the microstructure of the matrix and the particle incorporation of Ni–SiC– and Ni–TiO_2– composites. By electron backscattered diffraction data (EBSD), it has been shown that the typical columnar structure of pure Ni films is refined and nanoparticles are well dispersed in a matrix consisting of equiaxed grains. Fiber textures change from <211> to <110> in pure nickel due to sonication and to <100> and <111> due to nanoparticle incorporation under sonication. Later, Xia et al. [10] found de-agglomerated TiN particles (30 nm) in nanograined nickel by XRD, TEM, and AFM studies. Zheng et al. [11] applied ultrasound (0.7 W cm^{-2}) by a sonotrode, improving the dispersion and the content of the Al_2O_3 particles (11 wt.%) in a ZnNi matrix. As a result, the corrosion current decreased from 1.9×10^{-5} A cm^{-2} for ZnNi layers to 0.92×10^{-5} A cm^{-2} for ZnNi–Al_2O_3 composites and the hardness increased from 215 to 640 HV. Chang et al. [12] electroplated NiCo–Al_2O_3 composites, applying ultrasound with varying power from 64 to 160 W. Apart from texture changes (<111> and <100> to <110>), the content of Al_2O_3 in the composite decreased with rising power and the microhardness changed in particular due to the residual macrostress.

NiCo composites combine good mechanical and chemical properties with unique magnetic behavior. Thus, a variety of NiCo composite coatings have been examined, for example NiCo–SiC [13], NiCo–Si_3N_4 [14], NiCo–MoS_2 [15], and NiCo–diamond deposited from a Watts electrolyte [16], CoNi–nano-Al_2O_3 [17], and CoNi-$Fe_{12}O_{19}Ba_{0.2}Sr_{0.8}$ [18] using a sulfamate bath. Most of the results show the enhanced performance of the composite coatings. Al_2O_3 as a second phase is an economical and powerful material to strengthen composite coatings and to improve the corrosion and oxidation resistance [17, 19, 20], to enhance elastic properties [21], and to lower wear rates compared to pure nickel coatings [22]. Thus, NiCo–Al_2O_3 composites are functional layers with promising wear, friction, and corrosion behavior. An understanding of the correlation of the microstructure and the functional properties needs detailed studies which should not be done by inspecting only surface morphologies as mostly reported in the referenced papers [10–20].

The present study is focused on detailed microstructure studies of NiCo–Al_2O_3 composite coatings which have been co-deposited from sulfamate baths with different Co/Ni + Co ratios, constant particle bath loading and application of ultrasound. Cross-sections of composite layers are supposed to give clear evidence on particle distribution and grain size. The results of the XRD texture analysis using measurements with an Eulerian cradle and residual stress measurements are added and correlated to the tribological properties.

Experimental procedures

NiCo composite layers were electrodeposited from a sulfamate electrolyte. Analytical reagents and distilled water were used to prepare the plating solution. The plating bath for the preparation of the NiCo coatings was composed of 80 g/l $Ni(NH_2SO_3)_2{\cdot}4H_2O$ (Mathieu GmbH) and 2–12 g/l $Co(NH_2SO_3)_2{\cdot}4H_2O$ (Mathieu GmbH) for variating the Co/Ni + Co ratio. Forty grams per liter of H_3BO_3 (Merck Chemicals) was added as buffer; no surfactants were applied. For Al_2O_3 co-deposition, a bath loading of 50 g/l Al_2O_3 particles (diameter 250 nm, Saint Gobain) was used. The electrodeposition conditions were the following: cathode current density 2.5 A/dm^2, temperature 53–55°C, pH value 4.0–4.2, stirring speed 400 rpm. Ultrasound with a frequency of 35 kHz and a peak output of 240 W was applied in a heated ultrasound bath (Sonorex Super, Bandelin). Mild steel plates were used as the cathode substrate after degreasing and H_2SO_4 activation. A pure Ni plate served as the anode. Three samples per deposition condition were plated with a mean deposition rate of 0.4 μm/min up to a thickness of 70 μm.

The surface morphologies and cross-sections of the coatings were investigated with a scanning electron microscope (LEO 1455VP, Zeiss). The composition of the composite coatings was determined using an energy-dispersive spectrometer (EDS, EDAX) coupled with the SEM. EBSD (EDAX TSL) were collected in an FE-SEM (NEON 40 EsB, Zeiss) using the following parameters: 25 kV accelerating voltage, aperture 60 μm in high current mode, 50 nm step size. Texture and internal stress analysis was done on an X-ray diffractometer D5000 (Siemens) equipped with a CoKα source and an Eulerian cradle for detailed texture studies. The residual stresses of first order were determined from the strains measured by X-ray diffraction. Instrumented indentation tests (HM2000 XYm, HELMUT FISCHER GmbH) determined the indentation hardness as well as the elastic indentation modulus and the ratio of plastic deformability. Vickers hardness (HV0.05) was re-evaluated from this measurement according to ISO 14577–1:2002, appendix F. Additionally, Vickers hardness was measured additionally by a microhardness test device (DURAMIN, Struers). For both methods, ten measurements on cross-sections of each sample were conducted. The tribological properties of the coatings were evaluated as ball-on-disk tests conducting three measurements on each sample. The tests were carried

out against a hardened 100 Cr6 steel ball (θ 10 mm) at normal load of 10 N, a frequency of 1 s^{-1}, passing a testing distance of 100 m under unlubricated condition at room temperature and in ambient air. The wear volume was measured using a microoptical 3D measuring device (MicroCAD compact, GF Messtechnik GmbH).

Results and discussion

The variation of the plating conditions and the resulting compositions of the NiCo–Al_2O_3 composite coatings are summarized in Table 1 and Fig. 1. The composition of the metallic matrix has been changed by increasing Co $(NH_2SO_3)_2{\cdot}4H_2O$ concentration in the plating solution. Compared to the Co/Co + Ni ratio in the plating bath, the Co/Co + Ni ratio in the matrix of the composite layers is increased four times. This indicates that the less noble metal is preferentially deposited which is known as the anomalous type electrodeposition [22]. Due to the low Co content, the efficiency of the alloy deposition remains nearly constant. The mean deposition rate is 0.38± 0.01 μm/min for the Co/Co+Ni=0.1 regardless of sonication or silent deposition condition. The incorporation of the Al_2O_3 particles has been enhanced remarkably by application of ultrasound to the electrolyte during the co-deposition. It was possible to enhance the particle incorporation from 5 wt.% under silent condition to a threefold particle content in the matrix. With increasing cobalt content, the deposition rate is slightly increased up to 0.42±0.01 μm/min, and the particle content is marginally decreased from 15 to 12 wt.%.

The effects of ultrasound during electroplating and particle co-deposition are known as enhancing the species transport through the Helmholtz double layer, removal of hydrogen from the growing surface (thus decreasing matrix porosity), and particle dispersion. Sufficient particle incorporation requires an adequate ultrasound frequency and power since the cavitation bubbles should release enough energy for particle dispersion, but not too much energy for hindering particle incorporation. Comparable to counter-productive excessive bath agitating by stirring [17], reduced particle incorporation has been observed by excessive sonication [12]. The larger the bubbles, the more cavitation energy is released during implosion. Higher ultrasonic frequencies seem to be favorable because they generate smaller-sized cavitation bubbles per unit volume with lower energy but a larger number of bubbles. Otherwise, standing waves occur especially at higher frequencies and can result in failures such as streaks [23]. Therefore, an appropriate frequency has to be used and the applied; 35 kHz seem to be well suited to disperse and incorporate particles with diameters below 250 nm.

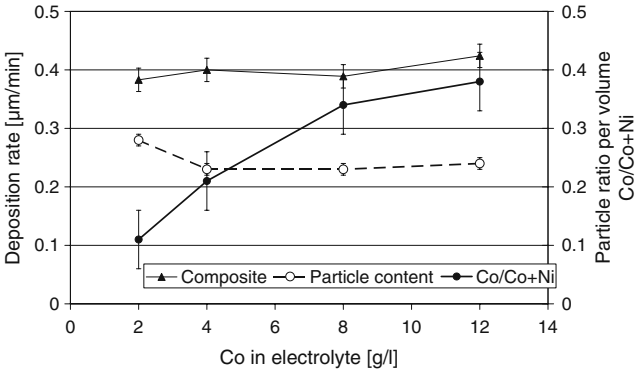

Fig. 1 Effect of the Co concentration in the electrolyte on the deposition rate of the composite (*filled triangles*), the particle content in the composite (*unfilled circles*), and the Co content in the matrix (*filled circles*)

In Fig. 2, the surface morphologies of a NiCo–Al_2O_3 composite coating prepared with 2 g/l $Co(NH_2SO_3)_2{\cdot}4H_2O$ under silent (Fig. 2a) and ultrasound conditions (Fig. 2b) are compared. The morphology of the latter is exemplary for all layers prepared with sonication of the electrolyte regardless of its composition. A relatively even surface with reduced nodular morphology is achieved compared to layers prepared under silent condition. Higher and uniform particle incorporation by electrolyte sonication can be assumed from the surface appearance. For confirmation

Table 1 Effect of the electrolyte composition and sonication on the layer composition

$Co(NH_2SO_3)_2{\cdot}4H_2O$ [g/l]	Co/Co + Ni in bath	Agitation	Co/Co + Ni in layer	Al_2O_3 content in wt.%
2	0.024	Silent	0.10	5
2	0.024	Ultrasound	0.11	15
4	0.048	Ultrasound	0.21	12
8	0.091	Ultrasound	0.34	12
12	0.130	Ultrasound	0.38	12

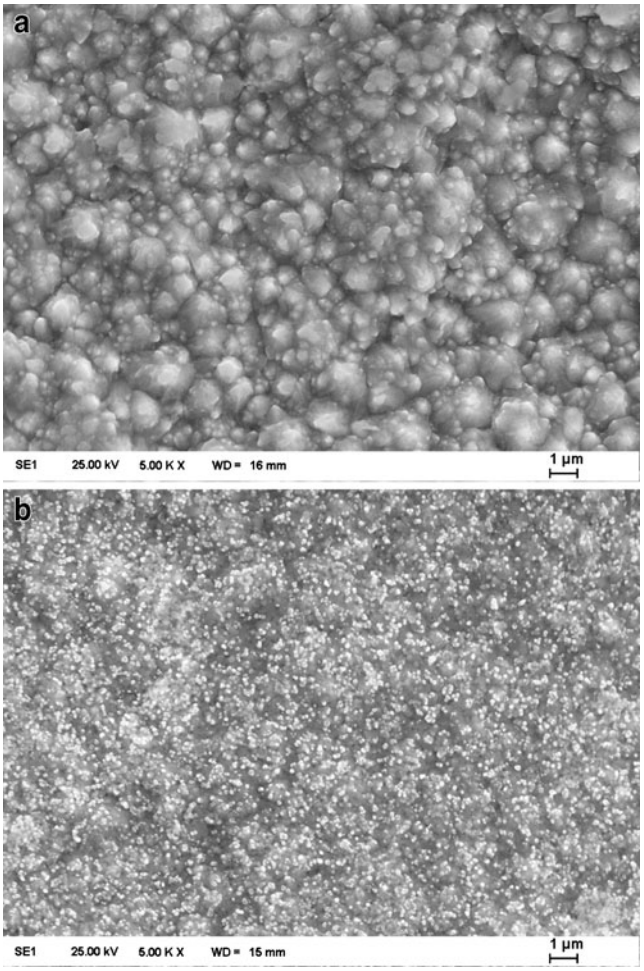

Fig. 2 Effect of ultrasound on the surface morphology of the NiCo–Al_2O_3 composite coating, **a** nodular under silent condition, **b** smooth under electrolyte sonication

and detailed examination, cross-sections of the layers are essential, thus providing appropriate conditions for EDS and EBSD measurements. The well-known agglomeration of sub-microscaled particles is shown for the composite plated under silent conditions (Fig. 3a). Such particle agglomerates do not disturb the columnar grain growth which is known as a typical feature of electroplated metallic layers for decades [24]. The application of ultrasound promotes a homogenous well-dispersed incorporation of particles, which seems to impede the growth of larger grains (Fig. 3b—the growth direction of the layer proceeds from bottom to top). This is observed in connection with a smoother surface for all samples regardless of the matrix composition.

The correlation between particle dispersion and grain-fining has been studied in detail by means of EBSD and parallel EDS. Figure 4 shows the quality maps of the diffraction patterns of the composite coatings near the substrate. The growth direction of the layer proceeds from right to left, i.e. the substrate is on the right in the maps. High pattern quality represented by bright regions is a result of good crystal orientation and low pattern quality represented by dark regions indicate low crystalline order such as in the grain boundaries. Under silent conditions, the grains grow columnar in the direction of the layer normal (Fig. 4a). The application of ultrasound causes a lower crystalline order in the grains, finer grains and a transition from columnar to equiaxial crystal growth (Fig. 4b). Reconstructed grain boundaries have been derived from the EBSD data, using a tolerance angle of 15° for the definition of the high-angle grain boundaries (HAGB). These HAGBs are presented together with the particle distribution for both types of NiCo–Al_2O_3 composite coatings with equal matrix composition but prepared under silent conditions (Fig. 5a) or under ultrasound conditions (Fig. 5b). The particle distribution has been revealed by a simultaneous EDS measurement of the aluminum signal, although to a limited extent due to the local EDS resolution.

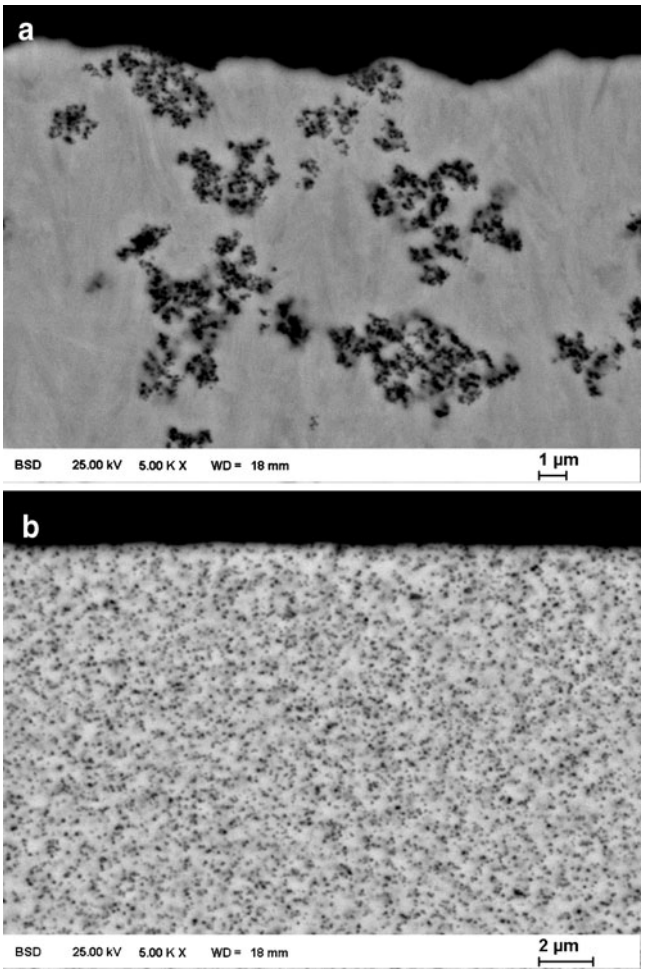

Fig. 3 Effect of ultrasound on the Al_2O_3 co-deposition, **a** agglomerated under silent condition, **b** well-dispersed under electrolyte sonication

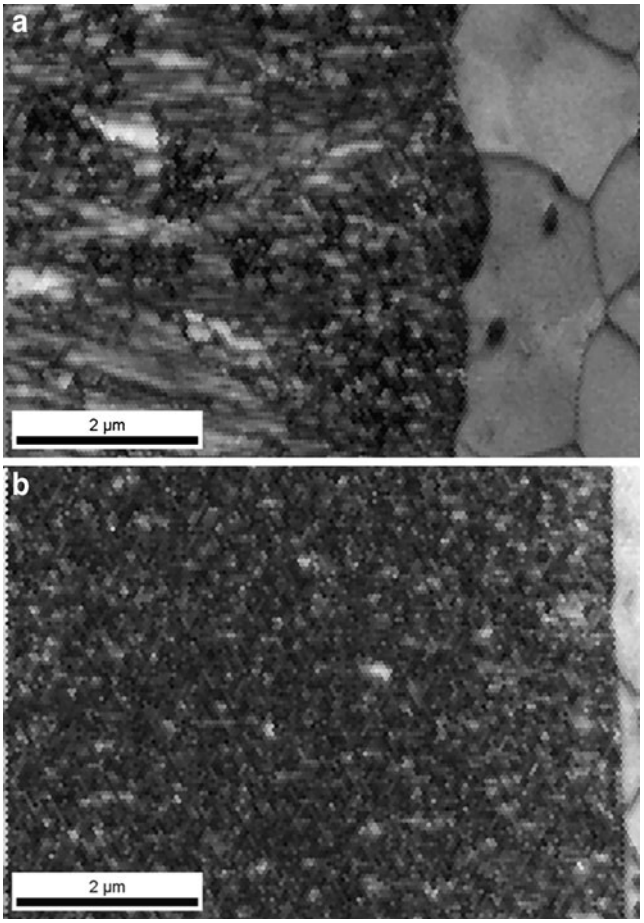

Fig. 4 EBSD pattern quality map of the composite cross-section, **a** silent condition, **b** electrolyte sonication

Both maps show that the high particle content is related to small grains in the matrix. Thus, composites with particle agglomerates show small grains only in these regions, and composites with well-dispersed and enhanced particle content show uniform grain-fining. The related size distribution of the grains is shown in Fig. 6, depicting a mean grain size diameter of 0.16±0.10 and 0.13±0.06 µm of the composite coatings prepared under silent and ultrasound conditions, respectively. The grains are not only smaller but also show a narrow distribution when deposited under ultrasonic agitation. Figure 7 shows the EBSD pole plots of the NiCo–Al_2O_3 composite coatings. Prepared under silent conditions, the metal matrix of the composite has a clear <110> fiber texture in growth direction (Fig. 7a), which is expected and regularly observed in electroplated layers [24, 25]. The texture has weakened and a strong <100> fiber texture has additionally developed during ultrasonically agitated deposition (Fig. 7b).

The microstructure changes described so far result in different mechanical properties of the composite layers (Fig. 8). The Vickers hardness is remarkably enhanced from 320 to 480 HV0.05 due to the well-dispersed particle incorporation. Moreover, the results of the instrumented indentation hardness test show a slightly decreased elastic indentation modulus. The subsequent, larger part of elastic deformation measured for the well-dispersed composite and considered by re-evaluating the Vickers hardness from the Martens hardness results in an even higher value. The hardness increase is expected because of grain refinement strengthening due to the Hall–Petch relationship and dispersion strengthening due to the Orowan mechanism.

The fiber texture evolution derived from EBSD in micron scale has been proved and confirmed by XRD for a representative area of some square millimeters. XRD examinations were done for all composite layers with varying cobalt content in the metallic matrix. It can be concluded from the phase analysis (Fig. 9) that in the examined cobalt ratio interval, the structure of the CoNi matrix is a solid solution of cobalt in nickel with a face-centered cubic structure and linear variation of the lattice

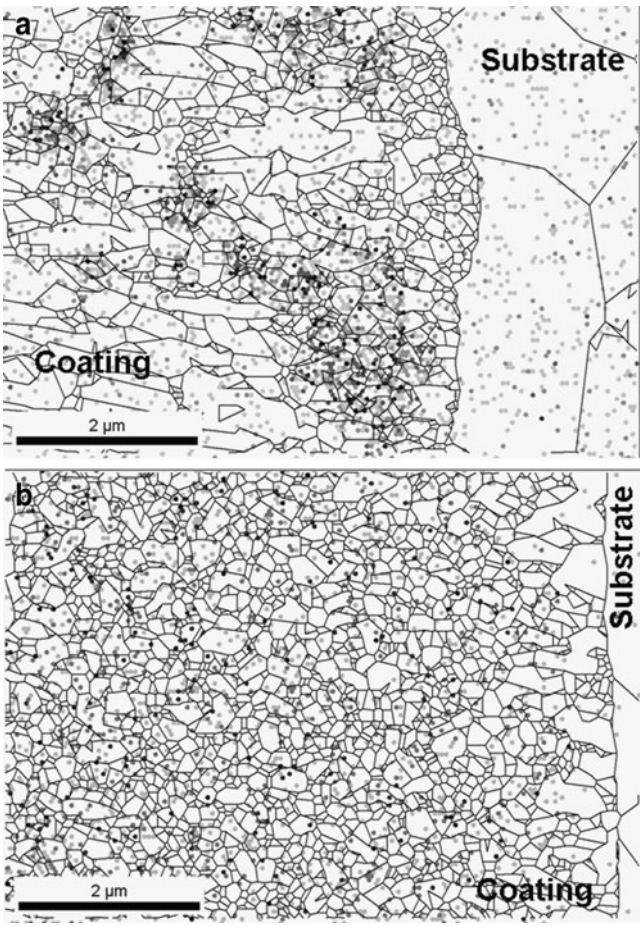

Fig. 5 Effect of ultrasound on the microstructure of the composite derived from EDS and EBSD, **a** large grains between agglomerated particles under silent condition, **b** fine grains due to particle dispersion under electrolyte sonication

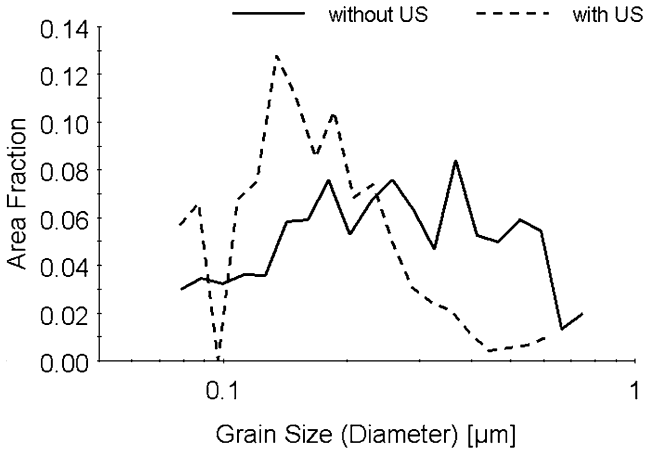

Fig. 6 Grain size distributions of the composite, **a** broad coarse-grained microstructure under silent condition, **b** narrow fine-grained microstructure due to particle dispersion

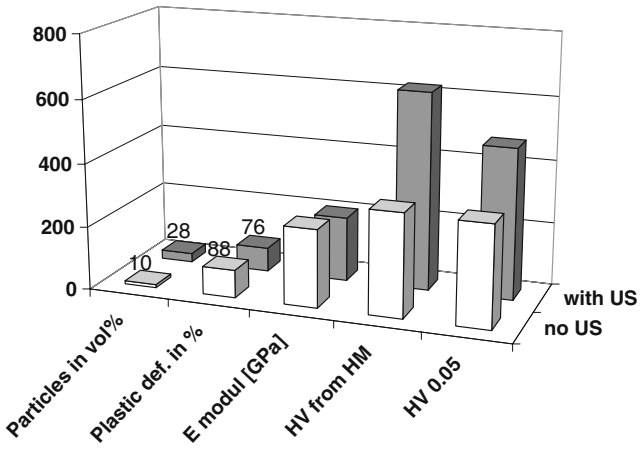

Fig. 8 Influence of well-dispersed particle incorporation (with US) on plastic deformability, elastic indentation modulus, and microhardness of the composite

parameter between 0.3523 and 0.3528 nm. The measured values are too small compared to the lattice constants of nickel (0.35280 nm, JCPDS No. 00-004-0850) and cobalt (0.354470 nm, JCPDS No. 00-015-0806) and the theoretical values calculated after Vegard's law for solid solutions (Fig. 10). The difference seems to be connected with the rather high lattice strains resulting in high tension stress values which are shown below. Additionally, the XRD phase analysis reveals some weak diffraction peaks of rhombohedral corundum attributed to the Al_2O_3 particles in the composite coatings (Fig. 9).

Texture analysis was done by measuring the intensity of the observed peaks under variation of the Euler angle ψ. The evaluation of the section through the pole figure, varying ψ between 0° and 70° regularly results in a weak <110> fiber texture in film growth direction for all composites. An exception is the composite prepared with the lowest Co concentration (2 g/l $Co(NH_2SO_3)_2{\cdot}4H_2O$)

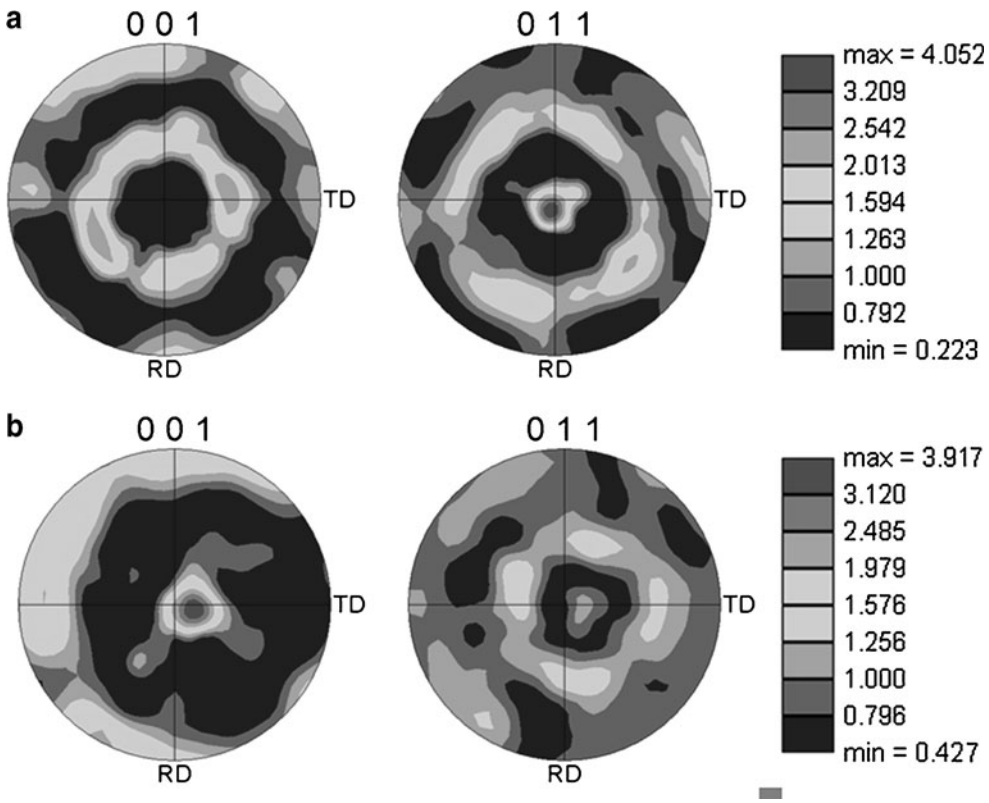

Fig. 7 Matrix texture in growth direction of the composite layer, **a** <110> fiber texture under silent condition, **b** additional <100> fiber texture under electrolyte sonication

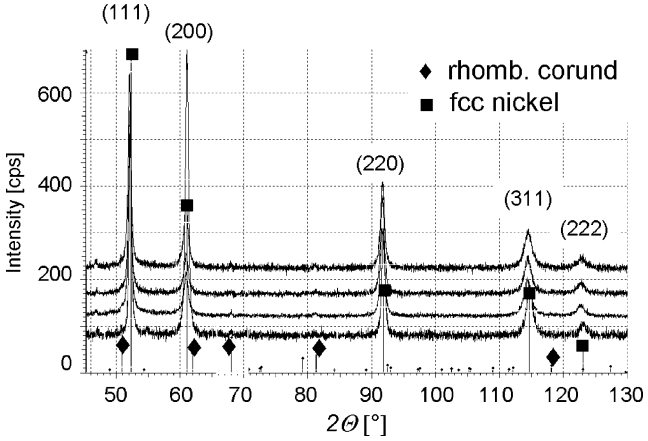

Fig. 9 Effect of the matrix Co/Ni + Co ratio (0.11–0.38 from bottom to top) on the XRD pattern of the composites with well-dispersed particle incorporation

and the highest particle content which shows a combination of <110> and <100> fiber textures corresponding to the EBSD results. Coherent crystal sizes have been derived from the peak broadening under consideration of the lattice strains using standardless crystallite size and strain analysis for calculation. The results derived from the {220} and the {111} peaks and summarized in Fig. 10. They show a variation between 15 and 30 nm with the higher values for low Co concentrations and lower lattice strains. Based on the measured lattice strains, the residual stresses of first order were determined (Fig. 11), which are rather high-tension stresses varying from 147 to 256 MPa with rising Co concentration in the solid solution. The cobalt concentration seems to be the influencing factor on the residual stress of the composites prepared under ultrasound.

The rising Co concentration in the composite matrix influences the Vickers hardness (re-evaluated from instrumented indentation measurements) as shown in Fig. 11. A

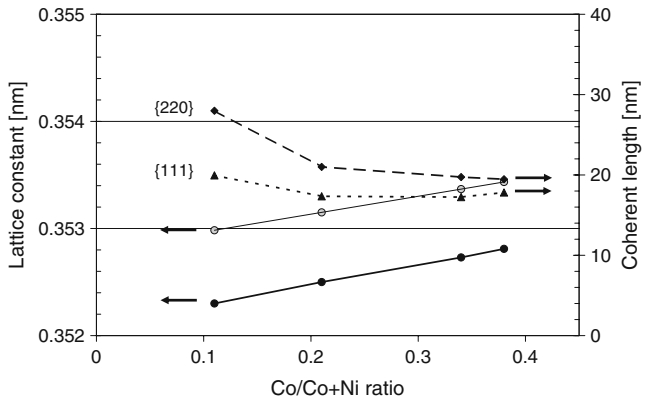

Fig. 10 Influence of the matrix composition on the coherent crystal size (*filled diamonds* {111} and *filled squares* {220}) and the lattice constants of the composite matrix (*filled circles* measured, *gray circles* calculated)

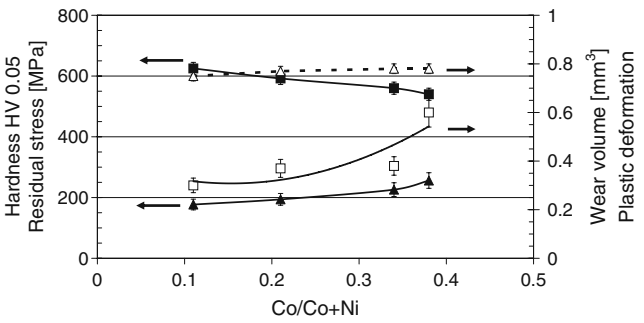

Fig. 11 Influence of the matrix composition on the plastic deformability (*unfilled triangles*), hardness (*filled squares*), residual stress (*filled triangles*), and wear (*unfilled squares*) of the composite layer

decrease has to be stated which is accompanied by a slight increase in plastic deformation. Moreover, the wear resistance decreases with rising Co concentration in the composite. The wear volume produced by the sliding wear of an unlubricated steel ball doubles in the concentration interval under investigation. In summary, the wear data show a correlation of the wear volume with the decreasing hardness and increasing first-order residual stress.

Apart from grain refinement and dispersion strengthening, an additionally expected solid-solution strengthening effect due to the rising Co concentration in the matrix is not found. Contrariwise, the wear resistance is decreased due to the rising first-order residual tensile stress in the matrix.

Conclusions

$NiCo–Al_2O_3$ composite coatings were electrodeposited under ultrasound conditions from nickel–cobalt sulfamate baths with a constant bath load of Al_2O_3 particles and varying cobalt concentration. Due to the low Co/Co + Ni ratio varied up to 0.4, the metallic matrix is a face-centered cubic nickel solid solution. The application of ultrasound to the plating bath enhances the particle co-deposition with appropriate dispersion. Thus, remarkable grain refinement is achieved and the Vickers hardness of the composites increases up to 50% by dispersion hardening. Due to the increase of the first-order residual stress in the matrix with increasing cobalt content in the nickel solid solution, no solid solution strengthening is observed. This shows that composite properties are determined by a complex of matrix properties with partially opposite effects which have to be taken into consideration.

Magnetic properties are very important in application of CoNi composites. A coercivity variation of the CoNi matrix with its typical soft-magnetic behavior can be assumed due to the ultrasound application and particle incorporation resulting in a variation of the grain size. This interesting question should be taken under consideration for future studies.

Acknowledgements The authors thank Mr. G. Röllig, Mr. E. Friesen, and Ms. C. Muhr for the materials tests, Ms. G. Fritsche for the XRD studies and especially her as well as Ms. G. Engelhardt for helpful discussions.

References

1. Müller Y, Schmutz P, Lampke T, Leopold A (2006) Metalloberfläche 60:40–42
2. Low CTJ, Wills RGA, Walsh FC (2006) Surf Coat Technol 201:371–383
3. Slipenyuk A, Kuprin V, Milman Y, Goncharuk V, Eckert J (2006) Acta Mater 54:157–166
4. Chwa SO, Klein D, Liao HL, Dembinski L, Coddet C (2006) Surf Coat Technol 200:5682–5686
5. Li WY, Zhang C, Liao HL, Li JL, Coddet C (2008) Surf Coat Technol 202:4855–4860
6. Feng QY, Li TJ, Teng HT, Zhang XL, Zhang Y, Liu CS, Jin JZ (2008) Surf Coat Technol 202:4137–4144
7. Chen L, Wang L, Zeng Z, Xu T (2006) Surf Coat Technol 201:599–605
8. Lampke T, Wielage B, Dietrich D, Leopold A (2006) Appl Surf Sci 253:2399–2408
9. Xia F, Wu M, Wang F, Jia Z, Wang A (2009) Curr Appl Phys 9:44–47
10. Zheng HY, An MZ (2008) J Alloys Compd 459:548–552
11. Chang LM, Guo HF, An MZ (2008) Mater Lett 62:3313–3315
12. Shi L, Sun CF, Zhou F, Liu WM (2006) Appl Surf Sci 252:3591–3599
13. Shi L, Sun CF, Zhou F, Liu WM (2005) Mater Sci Eng A 397:190–194
14. Shi L, Sun C, Liu W (2008) Appl Surf Sci 254:6880–6885
15. Sofer Y, Yarnitzkya Y, Dirnfeld SF (1990) Surf Coat Technol 42:227–236
16. Wu G, Li N, Zhou DR, Mitsuo K (2003) Surf Coat Technol 176:157–164
17. Cojocaru P, Spreafico M, Gomez E, Vallés E, Magagnin L (2010) Surf Coat Technol 205:195–199
18. Pushpavanam M, Manikandan H, Ramanathan K (2007) Surf Coat Technol 201:6372–6379
19. Ciubotariu AC, Benea L, Varsanyi ML, Dragan V (2008) Electrochim Acta 53:4557–4563
20. Wei X, Dong H, Lee CH, Jiang K (2008) Mater Lett 62:1916–1918
21. Gul H, Kilic F, Aslan S, Alp A, Akbulut H (2009) Wear 267:976–990
22. Brenner A (1963) Electrodeposition of Alloys, vol 2. Academic, New York, pp 246–297
23. Wu S, Leong T, Kentish S, Ashokkumar M (2009) J Phys Chem B 113:16568–16573
24. Fischer H (1954) Elektrolytische Abscheidung und Elektronenkristallisation in Metallen. Springer, Berlin
25. Lampke T, Steinhäuser S, Richter D, Wielage B (2007) Mat-wiss u Werkstofftech 38 1:23–31